Studies of nanotube-based resonant oscillators through multiscale modeling and simulation

Shaoping Xiao and Wenyi Hou
Department of Mechanical and Industrial Engineering and Center for Computer-Aided Design, The University of Iowa, Iowa City, Iowa 52242, USA
(Received 30 October 2006; published 12 March 2007)

We propose a multiscale method to study nanotube-based resonant oscillators. In the multiscale model, nanotubes are modeled via molecular dynamics, while the metal paddle is modeled as a rigid body. The molecular and continuum models are attached to each other through the interfaces on which carbon atoms are located. We employ the concepts of "virtual" atoms and bonds to effectively couple the molecular and continuum models. Using the proposed multiscale method, we investigate both linear and nonlinear characteristics of resonant oscillators. Effects of vacancy and temperature on mechanisms of oscillators are discussed.

DOI: 10.1103/PhysRevB.75.125414 PACS number(s): 85.35.Kt, 61.46.Fg

I. INTRODUCTION

Since carbon nanotubes have extraordinary mechanical and electrical properties,[1] they have been utilized as essential components in the design of novel nanoscale materials and devices. Tremendous molecular-dynamics simulations have been conducted to study the physical phenomena of nanotube-based composites and devices. Xiao and Hou[2] studied the mechanics of nanocomposites in which defected carbon nanotubes were embedded through molecular-dynamics simulations. Srivastava[3] employed molecular dynamics to discuss and test a phenomenological model for the rotational dynamics of a single laser-powered molecular motor that powered carbon nanotube-based gears. Molecular dynamics also assist researchers[4] to investigate the temperature-related energy dissipation of nanoscale devices. Recently, a new nanoscale device[5–7] in which an individual carbon nanotube serves as a torsional spring and mechanical support has been successfully fabricated. However, numerical modeling and studies of this device have not been reported.

Williams *et al.*[5,6] reported the fabrication of nanoscale mechanical devices incorporating multiwalled carbon nanotubes (MWNTs) as the torsional spring elements. They utilized electron-beam lithography to pattern a device element directly onto an individual MWNT on a silicon dioxide substrate. Consequently, the device consisted of a suspended lever, i.e., the "paddle," connected by an MWNT as a torsion beam. Papadakis *et al.*[7] used similar techniques to synthesize asymmetric oscillators that were also called resonant oscillators. The metal paddles in their experiments were not centered on the MWNTs, and the MWNTs were strained primarily in torsion. Once the paddle was given an electrostatic force, the oscillation was observed and the measured resonance frequencies were in the range of 1–9 MHz. Such oscillators can be used as sensors and clocks for high-frequency electronics. For example, with these nanoscale resonant oscillators, the clocks can be achieved with a single-stage device.[7] More recently, Meyer *et al.*[8] built a torsional pendulum with an individual single-walled carbon nanotube (SWNT), which was also used as a torsional spring and mechanical support for the metal paddle. They reported that this SWNT-based pendulum could be reproducibly turned to any position between 0° and almost 180°. All of the fabricated resonant oscillators described above had a paddle with a volume of about 0.04 μm^3 and a nanotube with a length of around 500 nm. Therefore, a molecular-dynamics model of such an oscillator may contain up to trillions of atoms and become infeasible for current computer resources.

Since molecular dynamics has limitations in simulating large nanosystems, multiscale methods are attractive to scientists and engineers. Recently developed multiscale modeling techniques have shown promise in treating phenomena at both nano- and larger scales. Multiscale methods can be divided into two classes: hierarchical multiscale methods and concurrent multiscale methods. Most hierarchical models contain a continuum approximation based on the properties of a subscale model, such as a molecular-dynamics (MD) model. The intrinsic properties of the material are determined at the atomic level and embedded in the continuum model according to a homogenization procedure.[9,10] However, the effects of defects cannot be considered with nanoscale continuum approximation. Concurrent multiscale methods[11–13] employ an appropriate model in which different methodologies are employed in each spatial scale simultaneously. The typical concurrent multiscale methods include the macroatomistic *ab initio* dynamics (MAAD) method[11] and the bridging domain coupling method.[12,13] They mainly coupled a continuum model (finite element methods) with a molecular model (molecular dynamics). Consequently, large models can be simulated without losing physical phenomenon details at the nanoscale.

In this paper, we develop a multiscale method that couples a continuum model and a molecular model to study the mechanical behavior of nanotube-based resonant oscillators. In the proposed multiscale model, the nanotube is modeled with molecular dynamics, while the metal paddle is modeled as a continuum. The edge-to-edge coupling technique[13] is employed in this multiscale method to efficiently attach the continuum model and the molecular model. Without losing accuracy, the metal paddle is treated as a rigid body since it has only small deformation during the torsional oscillation.

The outline of this paper is as follows. A multiscale modeling of nanotube-based resonant oscillators is proposed in Sec. II. The coupling of molecular dynamics and rigid body kinetics is introduced. In Sec. III, we discuss oscillation mechanisms of resonant oscillators that are linear oscillator

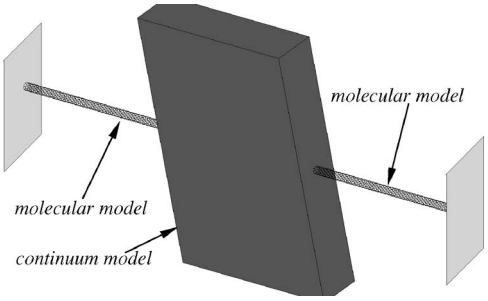

FIG. 1. Multiscale model of a nanotube-based resonant oscillator.

systems. The validation of the proposed multiscale method is conducted through comparing the experimental results with those predicted from multiscale simulations. Then, the nonlinear characteristics of resonant oscillators, including the effects of vacancy defects, temperature effects, and energy dissipation, are discussed in Sec. V, followed by the conclusions.

II. MULTISCALE MODELING

In a nanotube-based resonant oscillator, a part of the nanotube is embedded in the metal paddle. Since the metal paddle is mainly subject to rotation, it is modeled as the rigid body. Consequently, the embedded nanotube has nearly no deformation. Furthermore, we ignore the effect of the embedded nanotube on the angular moment of inertia of the metal paddle. Therefore, the nanotube in this oscillator can be viewed as two individual tubes connecting with the metal paddle, as shown in Fig. 1, which illustrates the multiscale model of a carbon nanotube-based resonant oscillator. In such a multiscale model, nanotubes are modeled via molecular dynamics in the molecular model Ω_M, while the metal paddle is treated as a rigid body in the continuum model Ω_C. We employ superscript and/or subscript M to denote the molecular model and C for the continuum model. The molecular and continuum models are attached to each other through the interfaces Γ_{int}. In this paper, we mainly consider the nanotubes on two sides of the metal paddle that have the same length.

Molecular model

In an isolated molecular model, the Hamiltonian H^M is given as

$$H^M[\mathbf{x}_I(t),\mathbf{p}_I^M(t)] = \sum_I \frac{1}{2m_I}\mathbf{p}_I^M \cdot \mathbf{p}_I^M + W^M[\mathbf{x}_I(t)], \quad (1)$$

where m_I is the mass of atom I, $\mathbf{x}_I$ is the position of atom I, $W^M(\mathbf{x})$ is the potential energy, which is the sum of the energies due to any force fields, and $\mathbf{p}_I^M$ is the momentum and is defined by

$$\mathbf{p}_I^M = m_I\dot{\mathbf{x}}_I = m_I\dot{\mathbf{d}}_I, \quad (2)$$

where $\mathbf{d}_I$ is the displacement of atom I. The total potential is computed as

$$W^M = -W_M^{ext} + W_M^{int} = -\sum_I \mathbf{f}_I^{ext}\mathbf{d}_I + \sum_{I,J>I} W_2(\mathbf{x}_I,\mathbf{x}_J) + \sum_{I,J>I,K>J} W_3(\mathbf{x}_I,\mathbf{x}_J,\mathbf{x}_K), \quad (3)$$

where the external potential energy W_M^{ext} is the work done by external forces $\mathbf{f}_I^{ext}$, such as electrostatic forces. The internal potential energy W_M^{int} describes the interatomic interactions. It includes W_2 and W_3, which are the potentials from pairwise and three-atom interactions, respectively. In addition, the Hamiltonian canonical equations of motion are given as

$$\dot{\mathbf{p}}_I^M = -\frac{\partial H}{\partial \mathbf{x}_I}, \quad \dot{\mathbf{x}}_I = \frac{\partial H}{\partial \mathbf{p}_I^M}. \quad (4)$$

Combining the above equations, we can obtain the equations of motion for molecular-dynamics simulation,

$$m_I\ddot{\mathbf{d}}_I = \mathbf{f}_I^{ext} - \frac{\partial W_M^{int}}{\partial \mathbf{x}_I}. \quad (5)$$

In this paper, we employ the modified Morse potential function, proposed by Belytschko *et al.*,[14] to describe the interaction between bonded carbon atoms. This potential can be written as

$$E = E_{stretch} + E_{angle},$$

$$E_{stretch} = D_e\{[1 - e^{-\beta(r-r_0)}]^2 - 1\},$$

$$E_{angle} = \frac{1}{2}k_\theta(\theta - \theta_0)^2[1 + k_s(\theta - \theta_0)^4], \quad (6)$$

where $E_{stretch}$ is the bond energy due to bond stretching or compressing, E_{angle} is the bond energy due to bond angle bending, r is the current bond length, and θ is the angle of two adjacent bonds representing a standard deformation measure in molecular mechanics. The parameters are

$$r_0 = 1.42 \times 10^{-10}\ \text{m}, \quad D_e = 6.031\,05 \times 10^{-19}\ \text{N m},$$

$$\beta = 2.625 \times 10^{10}\ \text{m}^{-1}, \quad \theta_0 = 2.094\ \text{rad},$$

$$k_\theta = 1.13 \times 10^{-18}\ \text{N m/rad}^2, \quad k_s = 0.754\ \text{rad}^{-4}. \quad (7)$$

It has been shown that this potential function results in reasonable Young's modulus and Poisson's ratio of nanotubes compared with experimental investigations.

Continuum model

In this paper, the axis of the nanotube is assumed to pass the centroid of the metal paddle. Since the metal paddle mainly has the motion of rotation and no deformation, it is treated as the rigid body in the continuum model. Then, the Hamiltonian H^C is given by

$$H^C = K^C + W^C = \frac{1}{2}J\dot{\theta}^2 + W^C, \quad (8)$$

where K^C is the total kinetic energy, J is the angular moment of inertia of the rigid body with respect to its rotational axis,

θ is the angular velocity, and W^C is the total potential energy, including strain energy (W_C^{int}) and the work done by external forces (W_C^{ext}),

$$W^C = -W_C^{ext} + W_C^{int}. \tag{9}$$

Since a rigid body has no deformation, its strain energy is zero. The external potential mainly results from interfacial loads due to the torsion of nanotubes. Therefore, the equation of motion for the rigid body rotation is

$$J\ddot{\theta} = T, \tag{10}$$

where T is the torque applied on the metal paddle. It has been observed that vertical deflections of nanotubes could be ignorable compared to torsional deflections.[7] In addition, we assume that the centroid of the metal paddle coincides with the nanotube axis. Therefore, the direction of the torque follows the nanotube axis, denoted by $\mathbf{e}_z$. The torque T is then computed as

$$T\mathbf{e}_z = \sum_I \mathbf{r}_I \times \mathbf{F}_I, \tag{11}$$

where $\mathbf{F}_I$ is the atomic force on atom I that is located at the interface between the nanotube and the metal paddle and $\mathbf{r}_I$ is the position vector of atom I with respect to the tube axis. Both $\mathbf{F}_I$ and $\mathbf{r}_I$ are projected on the x-y plane, while the tube axis follows the z axis. Then, the motion of the metal paddle can be determined via Eq. (10).

Molecular-continuum coupling

In this multiscale method, the carbon nanotubes are attached to the metal paddle without overlapping the subdomain except for the molecular-continuum interface. Since the modified Morse potential consists of the bond stretching energy and the bond angle-bending energy, simply gluing carbon atoms on the molecular-continuum interface will not account for the bond angle-bending energy between the nanotubes in the molecular model and the tube in the continuum model, although the tube in the continuum model is ignored because it has no deformation. In a manner similar to the edge-to-edge coupling technique,[13] we define two types of carbon atoms at the conjunctions between the continuum and molecular models: (1) "real" carbon atoms that are located on the interface and in the molecular model and (2) "virtual" carbon atoms that are located inside the continuum model. There are virtual bonds between real and virtual carbon atoms.

Figure 2 illustrates the molecular-continuum coupling technique utilized in the multiscale modeling of nanotube-based resonant oscillators. Although we mainly consider zigzag nanotubes in this paper, similar strategies can be conducted for nanotubes with other chiralities. In Fig. 2, real carbon atoms e, f, and g are in the molecular model. Among them, atom g is located at the continuum-molecular interface. Corresponding to atom g, there is a "virtual atom" h that is inside the continuum model. In addition, there is a "virtual" bond between atoms g and h.

Since the metal paddle is viewed as a rigid body, virtual bonds have no change in their length, so there is no bond stretching energy. However, the angles between virtual bonds and their neighboring bonds in the molecular model, e.g., the angles between bonds gh and ge/gf, as shown in Fig. 2, may change during the rotation of the metal paddle so that the bond angle-bending potential exists at the molecular-continuum interface. Such an angle-bending potential must be considered in molecular-dynamics simulations because it has effects on the atomic forces of carbon atoms that are on or close to the molecular-continuum interfaces. In the example shown in Fig. 2, those atoms include atoms e, f, and g. Consequently, the Hamiltonian of the whole system is written as

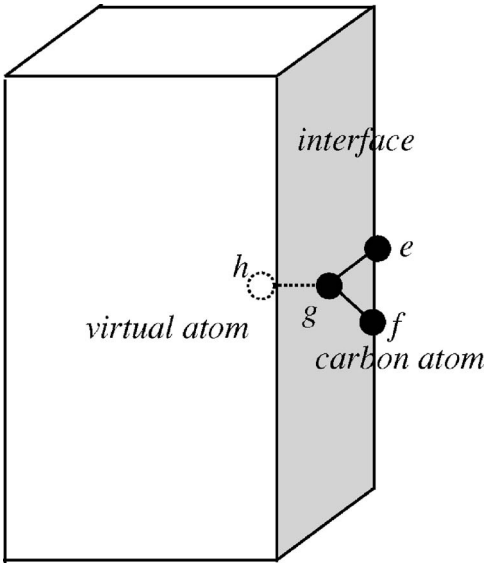

FIG. 2. The schematic diagram of virtual atoms and/or bonds at the interface.

$$H_{total} = H^M + H^C + E_{virtual}, \tag{12}$$

where H^M and H^C are the molecular and continuum Hamiltonians, respectively. $E_{virtual}$ is the potential due to angle change between the virtual bonds and other realistic bonds at the molecular-continuum interfaces. The equations of motion in the molecular and continuum models can be derived via the classic Hamiltonian mechanics. It should be noted that the equations of motion, i.e., Eq. (5), in molecular dynamics must be rewritten as

$$m_I\ddot{\mathbf{d}}_I = \mathbf{f}_I^{ext} - \frac{\partial(E + E_{virtual})}{\partial \mathbf{x}_I}, \tag{13}$$

where E is the potential of the tubes in the molecular model.

The nanotube and the rigid body are constrained on the interface Γ^{int} by

$$\mathbf{g}_I = \{g_{iI}\} = \{u_i(\mathbf{X}_I) - d_{iI}\} = 0 \tag{14}$$

where $\mathbf{X}_I$ is the position of atom I and $\mathbf{d}_I$ is the atomic displacement of atom I. In other words, the atomic displacements are required to conform to the continuum-level displacements at the positions of the atoms on the interface. Since the continuum model is a rigid body in this paper, we treat the entire metal paddle as an eight-node block element.

Then, the continuum-level displacements at the positions of the interfacial atoms and the virtual atoms can be calculated via the finite element approximation,

$$\mathbf{u}(\mathbf{X}_h) = \sum_{I=1}^{8} N_I(\mathbf{X}_h)\mathbf{u}_I, \tag{15}$$

where N_I represents the finite element shape functions at $\mathbf{x}_h$ and $\mathbf{u}_I$ represents the nodal displacements calculated from the rigid body rotation.

Multiscale simulation

At the beginning of a multiscale simulation, the metal paddle is given an initial angle of twist. Therefore, the displacements of atoms at the continuum-molecular interfaces and virtual atoms can be determined via Eqs. (14) and (15) as boundary conditions in the molecular model. Molecular-dynamics simulation in the molecular model is conducted through solving the equations of motion in Eq. (13). The Verlet velocity algorithm is employed as follows:

$$d(t+\Delta t) = d(t) + \dot{d}(t)\Delta t + \frac{1}{2}\ddot{d}(t)\Delta t^2, \tag{16}$$

$$\dot{d}(t+\Delta t) = \dot{d}(t) + \frac{1}{2}[\ddot{d}(t) + \ddot{d}(t+\Delta t)]\Delta t, \tag{17}$$

where Δt is the time step in molecular-dynamics simulation. In this paper, the time step is 1 fs. After updating atomic displacements of carbon nanotubes at each time step, we use Eq. (11) to calculate the torque acting on the metal paddle. Then, the rotation of the metal paddle can be determined by solving Eq. (10).

The above procedure can be iterated until the target time for output is reached. It should be noted that the calculation of the torque can be performed every several time steps to save computation time. However, in this paper we conduct it at each time step.

III. CHARACTERIZATION OF OSCILLATORS AS LINEAR OSCILLATION SYSTEMS

We first study mechanical behaviors of resonant oscillators as isolated systems with an initial temperature of zero. We also consider a small initial angle of twist, 10°, in this section. A resonant oscillator that contains two (9,0) tubes with a length of 4.12 nm connecting the metal paddle is investigated first. Each tube contains 360 carbon atoms. The material of the metal paddle is gold, which has a density of 19 300 kg/m^3. The dimensions of the metal paddle are as follows: length of 8 nm, width of 4 nm, and thickness of 2 nm. It should be noted that the metal paddle contained 4800 gold atoms. Consequently, the angular moment of inertia of the metal paddle is 0.007×10^{-36} kg m^2. Once the metal paddle is given an initial twist angle of 10°, the nanotubes are twisted. A torque is applied on the metal paddle due to the torsion of the nanotubes. After the metal paddle is released, it will rotate back and forth, and resonant oscillation can be observed. Figure 3 illustrates the configurations

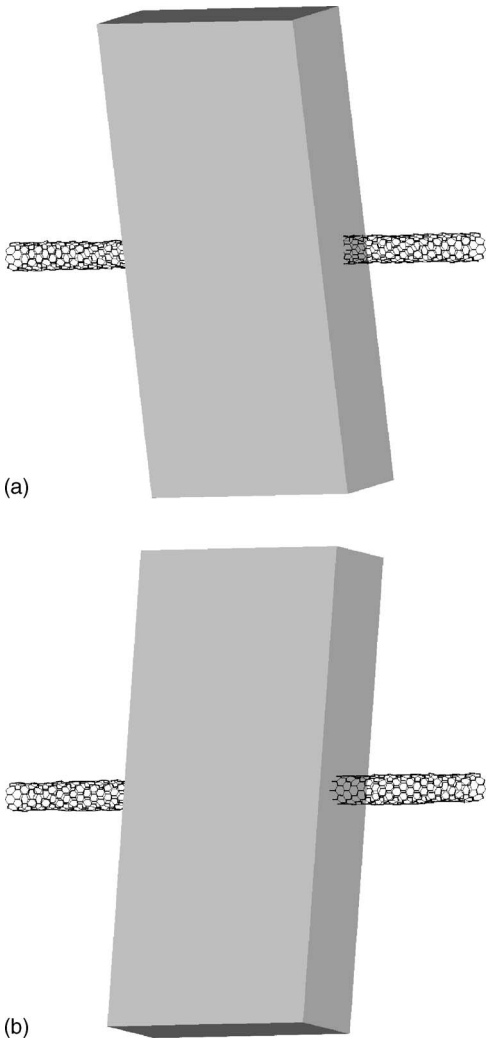

FIG. 3. Configurations of a nanotube-based resonant oscillator at (a) 0.5 ns and (b) 1.5 ns.

of this resonant oscillator at 0.5 and 1.5 ns, respectively. With the multiscale simulation, we obtained the evolution of angle change for the metal paddle, as shown in Fig. 4. It is evident that the resonant oscillation is stable and the calculated resonance frequency is 5.26 GHz.

We study the relationship between oscillators' resonance frequencies and the angular moments of inertia of the metal paddles. Four groups of resonant oscillators are considered,

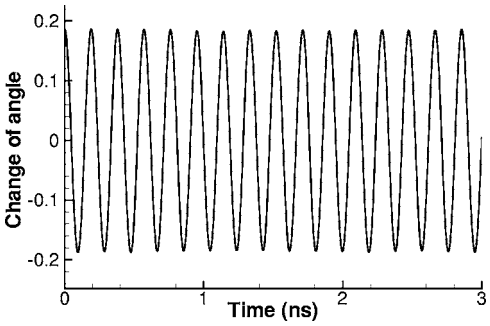

FIG. 4. Evolution of angle change of the metal paddle in the resonant oscillator.

TABLE I. Resonance frequencies with respect to different angular moments of inertia.

	J ($\times 10^{-36}$ kg m^2)			
Tubes utilized in the oscillators	0.144 (GHz)	0.072 (GHz)	0.036 (GHz)	0.009 (GHz)
(9,0)	1.19	1.68	2.38	4.76
(15,0)	2.60	3.66	5.21	10.4
(20,0)	4.00	5.66	8.02	16.0
(23,0)	4.85	6.85	9.68	19.3

and they contain (9,0), (15,0), (20,0), and (23,0) tubes, respectively. All the tubes have the same length, 4.12 nm, on both sides of the metal paddle. We vary the dimensions of the metal paddle so that angular moments of inertia J are in the range of 0.009×10^{-36}–0.144×10^{-36} kg m^2. Based on multiscale simulations, the resonance frequencies corresponding to the metal block's angular moments of inertia are summarized in Table I.

After studying the data in Table I, we found that the resonance frequency of a resonant oscillator is inversely proportional to the square root of the angular moment of inertia of the metal paddle once the utilized tubes remain the same. In other words, the following equation can be written as

$$f \propto \frac{1}{\sqrt{J}}, \tag{18}$$

where f is the resonance frequency. Such relationships are illustrated in Fig. 5 for all four groups of nanotubes studied in Table I.

We also found that the tube length is another major parameter to determine the resonance frequencies of nanotube-based resonant oscillators. Here, we chose (10,0) and (20,0) zigzag tubes with various tube lengths from 2 to 17 nm to conduct multiscale simulations. In the studied oscillators, the angular moments of inertia of the metal paddles remain 0.007×10^{-36} kg m^2. Similar to Fig. 5, Fig. 6 illustrates the following relationship between the resonance frequencies of

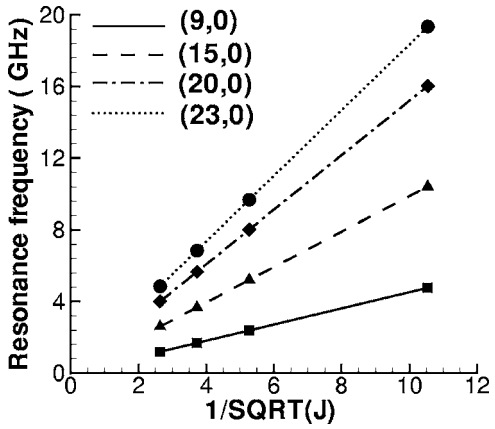

FIG. 5. Relationships between f and $1/\sqrt{J}$.

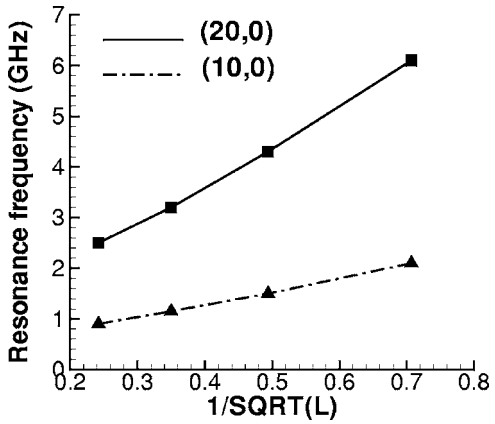

FIG. 6. Effects of tube length on resonance frequencies.

resonant oscillators and the lengths of the embedded tubes:

$$f \propto \frac{1}{\sqrt{l}}, \tag{19}$$

where l is the length of the tube embedded in the resonant oscillator.

Combining Eqs. (18) and (19), we can derive the following formula to predict the resonance frequency of oscillator 2, f_2, if the resonance frequency of oscillator 1, f_1, is known:

$$f_1 = \sqrt{\frac{J_2 l_2}{J_1 l_1}} f_2, \tag{20}$$

where l_1 and l_2 are the lengths of the embedded tubes, and J_1 and J_2 are the angular moments of inertia of the metal paddles in oscillators 1 and 2, respectively. It should be noted that the tubes had the same diameters and that we ignored the chirality effects.

The major computation time in the developed multiscale method is from molecular-dynamics simulation, since the metal paddle is modeled as a rigid body and has only small computation efforts. In the resonant oscillators fabricated in the literature,[5–7] the embedded nanotubes mostly contain up to millions of atoms. Obviously, molecular-dynamics simulations of those nanotubes are computationally intensive for a single personal computer. To save computation time and computer resources, the resonant oscillator contains a short tube, and a small metal paddle can be modeled to calculate the resonance frequency. Then, the frequencies of the corresponding resonant oscillators with long tubes and large metal paddles can be predicted via Eq. (20).

Indeed, it is known that the resonance frequency of a linear torsional oscillation system can be theoretically predicted via the following equation:

$$f = \frac{1}{2\pi}\sqrt{\frac{k}{J}}, \tag{21}$$

where k is the torsional stiffness of the embedded linear torsional spring and J is the angular moment of inertia of the metal paddle. We can see that Eq. (20) can be derived from Eq. (21), but calculation of the tube's torsional stiffness is not needed. On the other hand, we can say that our multi-

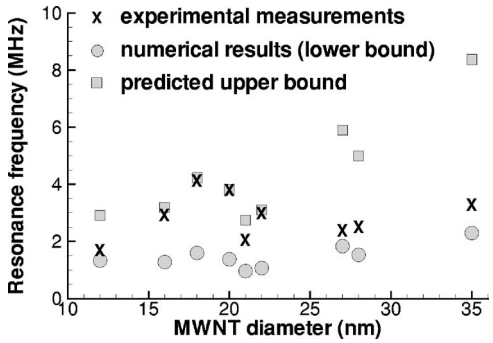

FIG. 7. Comparisons between experimental and semianalytical results.

scale method is verified by theoretical analysis by deriving Eq. (20) from Eq. (21).

IV. COMPARISON WITH EXPERIMENTAL OUTCOMES

Papadakis *et al.*[7] utilized MWNTs as the torsional springs to fabricate resonant oscillators. The measured resonance frequencies are in the range of 1.67–8.66 MHz. To validate the developed multiscale method, we simulate the devices listed in Table I of the work by Papadakis *et al.*[7] in this section and compare the calculated frequencies with the experimental outcomes. At first, we assume that only the outermost tube rotates during the motion of oscillators. Therefore, only the outermost tube instead of the whole MWNT is modeled in the molecular model. In Table I of Ref. 7, Papadakis *et al.* listed the diameter, torsional stiffness, and shear modulus of the MWNTs, and the measured resonance frequency for each resonant oscillator. Indeed, the MWNT torsional stiffness was calculated from the resonance frequency and the angular moment of inertia of the metal paddle, while the MWNT shear modulus was calculated from the MWNT's torsional stiffness, diameter, and length. Inversely, we can determine the angular moment of inertia of the metal paddle and the MWNT length for each device in Table I of Ref. 7. For each device, we simulate a corresponding small model using the multiscale method. The small model means that we use a small metal paddle and short single-walled nanotubes with the same diameter as the MWNT listed by Papadakis *et al.*[7] Then, we predict the resonance frequencies of the devices in the experiments via Eq. (20) and compare them with the experimental outcomes.[7] Figure 7 shows that although some resonance frequencies calculated from multiscale simulations compare well with the experimental measurements, all the numerical results are lower than the experimental measurements, especially for oscillators containing nanotubes with diameters in the range of 16–22 nm. This is because we model only the outermost tube and ignore the interlayer mechanical coupling in the MWNTs.

It has been known that the relationship between MWNT torsional stiffness (K) and its shear modulus (G) via the continuum mechanics model[15] is as follows:

$$K = \frac{\pi(d_{out}^4 - d_{in}^4)}{32l} G, \tag{22}$$

where d_{out} and d_{in} are the outer and inner diameters of the MWNT and l is the tube length. When we consider only the outermost shell of the MWNT, $d_{out}=d$ and $d_{in}=d-2t$, where d is the MWNT diameter listed in Table I of the work by Papadakis *et al.*[7] and t is the thickness of one nanotube layer, which is 0.34 nm. If the whole MWNT is taken as the torsional spring element, d_{in} is set as zero. Obviously, the calculated resonance frequency based on multiscale simulation is the least frequency that the simulated oscillator can have since only the outermost tube is modeled as the torsional spring element. Such a frequency is called the lower bound frequency for a resonant oscillator in this paper. Based on Eq. (21), the maximum resonant frequency, called the upper bound frequency here, that an oscillator can have when the whole MWNT acts as the torsional spring element is calculated as

$$f_{upper} = \sqrt{\frac{d^4}{d^4 - (d-2t)^4}} f_{lower}. \tag{23}$$

Figure 7 also shows that all the experimental outcomes are in the range from the lower bound frequencies to the upper bound frequencies. When the diameters of MWNTs are in the range of 16–22 nm, the experimental measurements are very close to the upper bound resonance frequencies, shown in Fig. 7. We can conclude that mechanical coupling in MWNTs plays a significant role during MWNT torsion in those devices.

V. NONLINEAR CHARACTERISTICS OF RESONANT OSCILLATORS

The advantage of our multiscale modeling method is that we can easily investigate nonlinear characteristics of resonant oscillators. In previous research,[16] a carbon nanotube has been observed to have a constant torsional stiffness within small angles of twist. If the angle of twist becomes larger, the nanotube's torsional stiffness gets smaller until the torsional buckling occurs. Therefore, we think that the resonance frequency of a resonant oscillator may decrease when the initial angle of twist is enlarged. For the resonant oscillator studied in Figs. 3 and 4, we consider the initial angle of twist in the range of 5°–55° in this section. We find that if the initial angle of twist is less than 15°, the resonance frequency becomes a constant of 5.26 GHz, as calculated from Fig. 4. When the initial angle of twist is enlarged to 30° and 55°, the resonant frequencies are dropped to 4.90 and 4.00 GHz, respectively, as shown in Fig. 8. We do not consider the occurrence of buckling in this paper. It should be noted that the relationship illustrated in Fig. 8 is for the resonant oscillator with a (9,0) tube with a length of 4.12 nm. The range for the angle of twist in which tubes can be employed as linear torsional springs varies for tubes with different sizes and lengths.

Obviously, the resonance frequencies of resonant oscillators as nonlinear systems can no longer be predicted via Eqs. (20) and (21). In this section, we also consider the effects of vacancy defects and temperature since they are significant to the mechanisms of nanoscale devices.

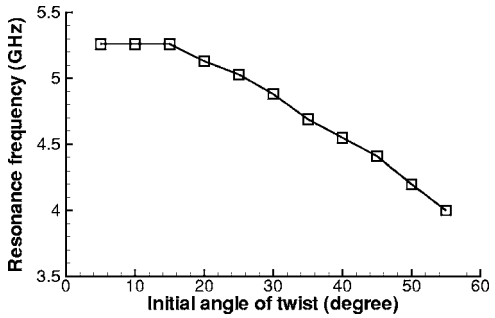

FIG. 8. Relationship of resonant frequencies and initial angles of twist.

Effects of vacancy defects

It has been shown that vacancy defects can dramatically reduce the stiffness, strength, and torsional stiffness of nanotubes.[16,17] Vacancy defects can be caused by ion irradiation, absorption of electrons, or nanotube fabrication processes. Such defects are modeled by taking out atoms, followed by bond reconstruction.[17] Vacancy defects can be classified as one-atom vacancy, two-atom vacancy, and cluster vacancy; details are provided by Hou and Xiao.[16] Two uncertainties associated with vacancy defects on nanotubes are considered in this paper. One uncertainty is the number of missing atoms and the other is the location of a vacancy defect. Due to the unique structures of single-walled carbon nanotubes, they can be mapped onto two-dimensional (2D) graphene planes with a thickness of 0.34 nm. Consequently, a three-dimensional (3D) model can be simplified as a 2D surface problem when considering vacancy defects on nanotubes. We employ a homogeneous Poisson point process to determine the occurrence probability of a specified number of Poisson points, i.e., missing atoms in this paper, via

$$P[N(A)=k]=\frac{e^{-\lambda A}(\lambda A)^k}{k!}, \quad k=1,2,3,\ldots, \tag{24}$$

where A is the plane area, $N(A)$ is the number of Poisson points (or missing atoms) on this area A, and λ is the Poisson point density (or missing atom density) per area. On the other hand, we assume that vacancy defects occur on carbon nanotubes in a completely random manner. For a given number of Poisson points, they are deposed on a two-dimensional

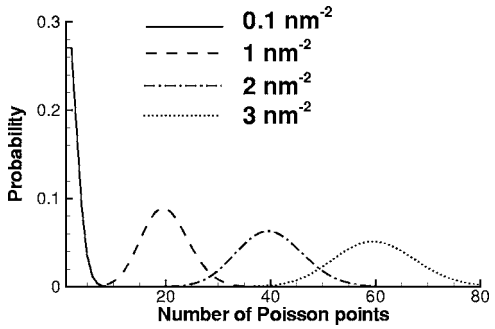

FIG. 9. Probability distributions of Poisson points at four missing atom densities.

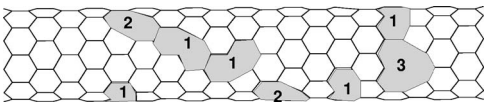

FIG. 10. The side view of a vacancy-defected (10,0) nanotube (1 represents the one-atom vacancy defect, 2 represents the two-atom vacancy defect, and 3 represents the cluster-atom vacancy defect).

graphene sheet, to which the considered nanotube can be mapped, at random positions. We mark the carbon atoms, which are those nearest to the Poisson points, as the missing atoms. After taking out the missing atoms, we perform bond reconstruction to generate one-atom, two-atom, and/or cluster-atom vacancy defects.

In this section, we choose (10,0) tubes with the length of 4.12 nm as torsional springs for nanotube-based resonant oscillators. The surface area of the carbon nanotube is 20.24 nm^2. The following missing atom densities are considered: 0.1, 1, 2, and 3 nm^{-2}. The probability distribution of the number of missing atoms for each missing atom density is shown in Fig. 9. In other words, the probability distribution in Fig. 9 determines the number of simulations for a specific number of missing atoms once the total number of simulations is given.

For a given number of missing atoms, the vacancy defects will be randomly located as described above. Figure 10 illustrates the side view of a vacancy-defected (10,0) nanotube. We can see that there are five one-atom vacancies, two two-atom vacancies, and one cluster-atom vacancy. Obviously, for the same number of missing atoms, the numbers and locations of vacancy defects can vary from case to case.

We conduct 100 simulations for each given missing atom density to investigate the statistical properties of the resonance frequencies when the resonant oscillators contain vacancy-defected nanotubes. All metal paddles have the angular moment of inertia of 0.0237×10^{-36} kg m^2 in the studied resonant oscillators. Figure 11 shows the relationship between the resonance frequency and the missing atom density on the carbon nanotube surface. Due to uncertainties of vacancy defects, the resonance frequencies follow the Gaussian distribution. We can see that on average a larger missing atom density results in a lower resonance frequency since the nanotube with more missing atoms generally has less torsional stiffness. However, due to the uncertainties of vacancy defects, it is possible that a resonant oscillator embedding a

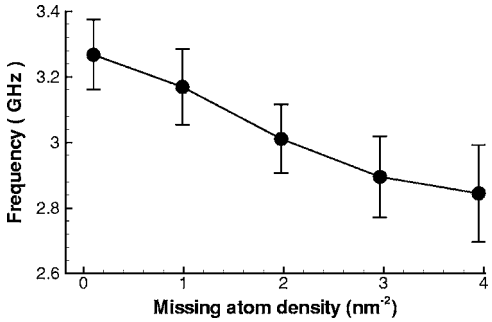

FIG. 11. Vacancy defect effects on the resonant frequency.

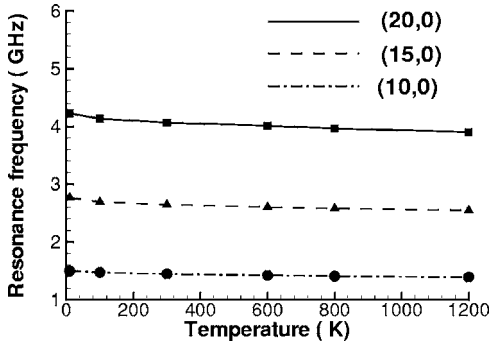

FIG. 12. Temperature effects on resonant frequency.

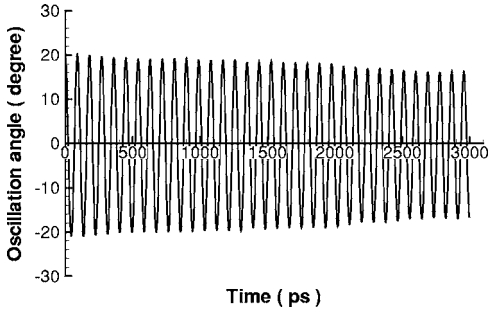

FIG. 13. Illustration of oscillation angle at room temperature of 300 K.

nanotube with more missing atoms has a higher resonance frequency.

Effects of temperature and energy dissipation

Temperature effects, including energy dissipation at finite temperatures, are usually significant to the mechanisms of nanoscale devices.[4] We first investigate the temperature effects on the resonance frequencies of carbon-nanotube (CNT)-based resonant oscillators at finite temperatures. Three types of nanotubes, (20,0), (15,0), and (10,0), are employed as torsional spring elements in oscillators. The length of all of these tubes (on each side of the metal paddle) is 8.236 nm. The metal paddle is made of gold, and its dimensions (length, width, and height) are 14, 2, and 14 nm. The angular moment of inertia of the metal paddle with respect to the rotation axis is $J=0.126\times10^{-36}$ kg m^2.

During the multiscale simulation, the Hoover thermostat[18] is applied in the molecular model to maintain nanotubes at a desired temperature. The initial rotation angle is set to be 10°. Figure 12 shows the resonance frequencies of the oscillators mentioned above at various temperatures, including 10, 100, 300, 600, 800, and 1000 K. We can see that the temperature effects on the resonance frequencies are slightly significant, e.g., a higher temperature results in a lower resonance frequency. The reason is that nanotubes have lower torsional stiffness at higher temperatures.

Energy dissipation is a critical issue for nanoscale devices at finite temperatures because it determines the quality factor of devices. The quality factor is defined as the inverse of the energy dissipation, which is a measure to estimate how much energy can be recovered. Although finite temperatures have slight effects on the resonance frequency of a resonant oscillator, energy dissipation does exist. Here, we consider a resonant oscillator containing (10,0) tubes with a length of 4.12 nm on each side of the metal paddle, whose angular moment of inertia is $J=0.002\times10^{-36}$ kg m^2. The resonance frequency of this oscillator is 5.53 GHz. Figure 13 illustrates that the oscillation angle decreases when the oscillator is at 300 K. In other words, the energy dissipation exists, and we believe that the oscillator will decay away eventually.

We next investigate energy dissipation of resonant oscillators with various resonance frequencies. In those oscillators, the same (10,0) nanotubes with the length of 4.12 nm are employed. We vary the dimensions of the metal paddles so that various resonance frequencies can be achieved. Figure 14 illustrates energy dissipation of resonant oscillators with various frequencies at the room temperature of 300 K. It is evident that larger energy dissipation occurs in the resonant oscillator with higher resonance frequency. In other words, the nanotube-based resonant oscillator that has a lower resonance frequency has a higher quality factor.

VI. CONCLUSIONS

In this paper, we proposed a multiscale method to model and study nanotube-based resonant oscillators. We found that if a small angle of twist was given to the metal paddle, oscillators would act as linear oscillator systems. We mostly modeled the outermost tube of the MWNT that was utilized as a spring element in a resonant oscillator. Considering mechanical coupling between interlayer tubes in the MWNT, we could provide a range of resonance frequencies via multiscale simulation for a studied oscillator, and the experimental measurements fell into such ranges. In addition, the proposed multiscale method had advantages in simulating nonlinear characteristics of resonant oscillators, such as when initial angles of twist were large, when nanotubes had vacancy defects, and when oscillators were at finite temperatures. The conclusion is that larger initial angles of twist resulted in lower resonant frequencies. On average, more vacancy defects on the nanotube resulted in lower resonant frequencies. Although temperature effects were found to have only slight effects on the resonant frequencies of oscillators, energy dissipation did exist, and the oscillator would finally cease. Oscillators having lower resonance frequencies

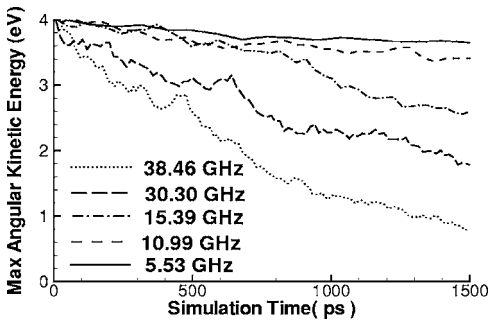

FIG. 14. Effects of high frequency on energy dissipation rate.

had lower energy dissipate rates, i.e., higher quality factors. The issue of energy dissipation should be considered when designing nanoelectromechanical systems utilizing nanotube-based resonant oscillators.

It should be noted that it was possible to simulate half of the resonant oscillator systems since the systems simulated in this paper were symmetric. However, if the metal paddle does not attach to the center of the carbon nanotube, the whole system must be modeled. On the other hand, we only consider SWNTs in this paper. The MWNT-based resonant oscillators can also be simulated via the proposed multiscale method. Such modeling and simulation will be our future research.

ACKNOWLEDGMENTS

We acknowledge support from the Army Research Office (Contract No. W911NF-06-C-0140) and the National Science Foundation (Grant No. 0630153).

[1] V. N. Popov, Mater. Sci. Eng., R. **43**, 61 (2004).
[2] S. Xiao and W. Hou, Phys. Rev. B **73**, 115406 (2006).
[3] D. Srivastava, Nanotechnology **8**, 186 (1997).
[4] S. Xiao, D. Andersen, R. Han, and W. Hou, J. Comput. Theor. Nanosci. **3**, 142 (2006).
[5] P. Williams, S. Papadakis, A. Patel, M. Falvo, S. Washburn, and R. Superfine, Phys. Rev. Lett. **89**, 255502 (2002).
[6] P. Williams, S. Papadakis, A. Patel, M. Falvo, S. Washburn, and R. Superfine, Appl. Phys. Lett. **82**, 805 (2003).
[7] S. J. Papadakis, A. R. Hall, P. A. Williams, L. Vicci, M. R. Falvo, R. Superfine, and S. Washburn, Phys. Rev. Lett. **93**, 146101 (2004).
[8] J. Meyer, M. Paillet, and S. Roth, Science **309**, 1539 (2005).
[9] E. Tadmor, R. Phillips, and M. Ortiz, Int. J. Solids Struct. **37**, 379 (2000).
[10] S. Xiao and W. Yang, Comput. Mater. Sci. **37**, 374 (2006).
[11] F. Abraham, J. Broughton, N. Bernstein, and E. Kaxiras, Europhys. Lett. **44**, 783 (1998).
[12] S. Xiao and T. Belytschko, Comput. Methods Appl. Mech. Eng. **193**, 1645 (2004).
[13] T. Belytschko and S. Xiao, Int. J. Multiscale Comp. Eng. **1**, 115 (2003).
[14] T. Belytschko, S. P. Xiao, G. C. Schatz, and R. S. Ruoff, Phys. Rev. B **65**, 235430 (2002).
[15] W. C. Young, *Roark's Formulas for Stress and Strain* (McGraw-Hill, New York, 1989).
[16] W. Hou and S. Xiao, J. Nanosci. Nanotechnol. (unpublished).
[17] S. Mielke, D. Troya, S. Zhang, J. Li, S. Xiao, R. Car, R. Ruoff, G. Schatz, and T. Belytschko, Chem. Phys. Lett. **390**, 413 (2004).
[18] W. G. Hoover, Phys. Rev. A **31**, 1695 (1985).